Scientific Reports

https://doi.org/10.1038/s41598-026-35215-z

Article in Press

Discrete thermal analysis of the E–type shell–and–tube heat exchanger

Received: 28 October 2025

Accepted: 3 January 2026

Published online: 15 January 2026

Cite this article as: Bayramoğlu K., Kaya I. & Ust Y. Discrete thermal analysis of the E–type shell–and–tube heat exchanger. *Sci Rep* (2026). https://doi.org/10.1038/s41598-026-35215-z

Kubilay Bayramoğlu, Ibrahim Kaya & Yasin Ust

We are providing an unedited version of this manuscript to give early access to its findings. Before final publication, the manuscript will undergo further editing. Please note there may be errors present which affect the content, and all legal disclaimers apply.

If this paper is publishing under a Transparent Peer Review model then Peer Review reports will publish with the final article.

ARTICLE IN PRESS

© The Author(s) 2026. **Open Access** This article is licensed under a Creative Commons Attribution-NonCommercial-NoDerivatives 4.0 International License, which permits any non-commercial use, sharing, distribution and reproduction in any medium or format, as long as you give appropriate credit to the original author(s) and the source, provide a link to the Creative Commons licence, and indicate if you modified the licensed material. You do not have permission under this licence to share adapted material derived from this article or parts of it. The images or other third party material in this article are included in the article's Creative Commons licence, unless indicated otherwise in a credit line to the material. If material is not included in the article's Creative Commons licence and your intended use is not permitted by statutory regulation or exceeds the permitted use, you will need to obtain permission directly from the copyright holder. To view a copy of this licence, visit http://creativecommons.org/licenses/by-nc-nd/4.0/.

ARTICLE IN PRESS

Discrete thermal analysis of the E–type shell–and–tube heat exchanger

Kubilay Bayramoglu[1], Ibrahim Kaya[*2], Yasin Ust[2],
[1]Zonguldak Bulent Ecevit University, Department of Mechanical Engineering, Zonguldak, Türkiye

[2]Yıldız Technical University, Department of Naval Architecture and Marine Engineering, İstanbul, Türkiye

* Corresponding author: ibrkaya@yildiz.edu.tr

Abstract

Thermal analysis of heat exchangers is crucial in both conventional and sustainable energy systems. However, traditional (non–dimensional) methods may be inadequate in certain scenarios, such as temperature or heat maps, pinch point prediction, two–phase flows, or trans–critical flows. These challenges can be addressed using discrete thermal analysis methods, which allow for the numerical calculation of temperature and heat maps, or effectiveness values for heat exchangers having any complex flow patterns. This research introduces the Discrete Sub–Heat Exchanger (DSHE) method and demonstrates its application to the E–type shell–and–tube heat exchangers under defined NTU and Cr conditions. According to the application results, temperature and heat maps have been calculated successfully, with numerical effectiveness values closely matching analytical ones. Finally, sensitivity and error analyses in wide NTU and Cr ranges confirm the excellent applicability of the DSHE method with analytical error rates.

Keywords: Discrete thermal analysis, discretization of heat exchangers, temperature profiles, heat distribution, numerical effectiveness, numerical heat exchanger thermal modeling

ARTICLE IN PRESS

ARTICLE IN PRESS

1. Introduction

The heat exchangers constitute essential components in a wide range of industrial applications, including power generation, process engineering, marine systems, and emerging sustainable energy technologies. Accordingly, numerous heat exchanger configurations and heat sink designs have been proposed in the literature to enhance thermal performance and operational efficiency. For example, to improve the performance of the heat sink, the phase change materials were investigated experimentally [3] and numerically [4]. The use of vibration as an active method for heat transfer enhancement in heat exchangers has attracted attention in the literature [5], [6], [7], [8], [9]. For the heat exchangers, another way to improve the performance of heat exchangers is to develop different flow patterns. Therefore, numerous flow patterns exist, and many studies have been conducted in the literature to enable dimensionless thermal analysis of these flow patterns.

The non–dimensional thermal analysis methods are practical approaches used to predict the thermal performance of the heat exchangers, mostly in single–phase flows. The most widely used of these methods can be considered as the log–mean temperature difference (LMTD) and the effectiveness–transfer unit number (ε–NTU) methods. These methods have the triple dimensionless number groups and the heat exchanger's outlet temperatures or heat transfer surface areas can be calculated by using these number groups, with some simplifications.

The ε–NTU method was first formally introduced by Kays and London [1] in 1950 and it can be considered as a variant of the thermal effectiveness–transfer unit number (P–Ntu) method [2]. Since the ε–NTU method have this dual calculation methodology for defined area or temperature conditions, it has superiority over the LMTD method [2]. Because of including outlet temperatures in the heat transfer equation of the LMTD method, even at constant fluid properties, iterations are required in heat exchanger thermal analyses at defined area condition.

The configurations of the E–type shell–and–tube heat exchangers (E–type STHEs), most commonly encountered in applications, classified by Tubular Heat Exchanger Manufacturers Association (TEMA) [10] are shown in Fig. 1 with varying numbers of tube passes (*Np*). It is important to note that the flow pattern within the E–type STHEs changes with *Np*, thereby necessitating distinct the ε–NTU relations or a set of curves to ensure accurate thermal analysis. Moreover, the analytical derivation of the ε–NTU relationships becomes more difficult as the number of tube passes increases. Sekulic et al. [11] reviewed and classified in detail the methods used to derive the correction factor and effectiveness relations used in many flow patterns. According to the authors, these approaches are classified as analytical, semi–analytical, numerical, matrix formalism, and chain rule methods. Within the scope of this research, the main studies in the literature related to these methods for the E–type STHEs are given below.

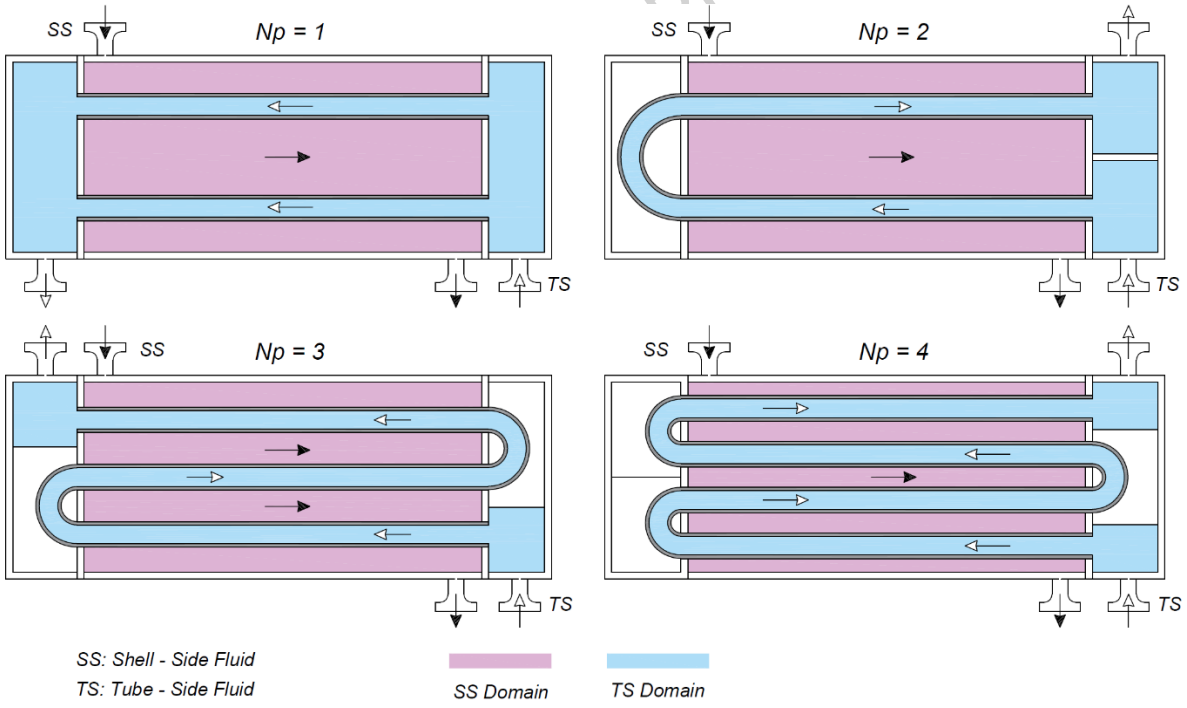


Fig. 1 The E–type shell–and–tube heat exchangers

Underwood [12] derived true mean temperature difference relations for the E–type STHEs having two and four–tube passes by solving the integral

ARTICLE IN PRESS

equations [11]. Similarly, Nagle [13] also derived and presented the relations of correction factors for the E–type STHE having two, four and six–tube passes by solving integral equations. Afterwards, Nagle [13] also derived and presented the correction factor of the E–type STHE having four–tube and two–shell passes at overall counter–flow. Kern [14] also clearly showed the derivation of correction factor for the E–type STHE having two–tube passes by solving the second order differential equation system. Fisher [15] derived the implicit analytical relation of true mean temperature difference for the E–type STHE having three–tube passes at overall counter–flow, unlike other authors. The author also presented the tables and graphs of the correction factor for this flow pattern. At the end of this work, Fisher [15] presented the correction factor graphs for three–tube and two, three and four–shell passes heat exchanger configurations in overall counter–flow. Yendall presented an implicit form for the correction factor relation of the E–type STHE having four–tube passes to Bowman et al. [16]. These authors used analytical methods to derive the correction factors for E type STHEs having different numbers of tube passes.

The ε– NTU relations of parallel and counter–flow pattern, the basic flow–pattern types, were derived by solving the integral equations [17], [2]. Effectiveness relation of the E–type STHEs having any even number of tube passes, by solving the second order differential equation system, was derived by Kern and Kraus [18]. Baclic [19] showed that by limiting the number of tube passes to infinity in the relation derived by Kern and Kraus [18], thermal effectiveness relations of this heat exchanger type are equivalent to both mixed cross–flow heat exchangers. Moreover, Baclic [20] derived the thermal effectiveness relations of the E–type STHEs having an odd number of tube passes' overall counter–flow and parallel–flow using the algebraic operations used by Seban [21]. Pignotti and Tamborenea [22] derived thermal effectiveness relations for the E–type STHEs having arbitrary numbers of tube and shell passes. The authors used a two–stage solution method and in the

ARTICLE IN PRESS

first step, just like Baclic [20], they used the algebraic method to obtain the thermal effectiveness relations of the E type STHEs having single shell and arbitrary number of tube passes. In the second step, the authors obtained thermal effectiveness relations, which also takes into account an arbitrary number of shell passes by using Domingos' matrix method [23]. Domingos [23] developed the Matrix Formulation to derive the effectiveness relation of the counter, parallel and more complex heat exchanger networks. Further to Matrix Formulation, Pignotti [24] developed Generalized Matrix Formalism for thermal effectiveness relation of the E–type STHEs having finite number of baffles.

In numerical methods, Crozier and Samuels [25] brought out correction factor values depending on thermal effectiveness and thermal capacity ratio for the E–type STHEs having three tube passes by using Runge–Kutta method iteratively. The authors confirmed their results with the values predicted by Nagle's results [13]. Hess [26] carried out a thesis study to derive the numerical effectiveness relations of the E type STHEs having an odd number of tube passes. The author presented effectiveness tables and polynomial regression coefficients for three and five–tube passes in the overall counter and parallel flows. Gaddis and Schlünder [27] have introduced a general discrete method to determine the effect of the baffles on effectiveness of the E–type STHEs having multi tube passes by assuming cross flow between baffles. Ribando et al. [28] performed one and two dimensional discrete thermal analyses of the E–type STHE having two–tube passes to obtain temperature profiles of the heat exchanger. The authors discretized the heat exchanger in sub–heat exchangers and applied the mean temperature difference method. They also defined *Nodal Connectivity* to describe the relationship between the node temperatures.

While deriving the effectiveness relations of any flow pattern, the fluid properties are considered constant throughout a heat exchanger. However, the fluid properties change also with the changing enthalpy and pressure of

ARTICLE IN PRESS

the fluids. To overcome this problem, Karellas et al. [29], discretized the plate heat exchanger in trans–critical flow into N number of sub–heat exchangers with the equal thermal load and performed heat exchanger sizing by LMTD method iteratively. Cayer et al. [30] sized the counter flow heat exchangers in trans–critical CO2 Rankine cycle by using the discrete method proposed by Karellas et al [29]. Dai et al. [31] sized the counter flow heat exchangers in two–phase flow for Organic Rankine cycle and trans–critical flow for CO_2 Rankine cycle by using the same proposed discrete method. Moreover, unsteady heat conduction and axial heat transfer along the tube can also be modeled using numerical methods. Bracco et al. [32] performed discrete thermal analyses of a counter–flow heat exchanger, which is oil cooler, for both steady and unsteady cases. The authors considered the solid–state energy storage in the shell and tube walls, which are the heat exchanger structural parts, in the heat transfer equations.

Although Karellas et al. [29] declared that the ε–NTU method cannot be used in discrete thermal analyses of heat exchangers, Nellis and Klein [33] proposed the discrete method using the ε–NTU method for thermal analysis of a parallel flow plate heat exchanger at defined area condition. This discrete method discretizes a heat exchanger into N number of sub–heat exchanger pairs. For each sub–heat exchanger, the ε–NTU method is applied in an iterative manner till convergence is achieved, except for parallel–flow pattern. Moreover, the method proposed by Karellas et al. [29] is only applicable to the heat exchangers having single–fluid pass.

In this research, the discrete thermal analysis methodology introduced by Nellis and Klein [33] is adapted and applied to E_2 STHE due to E_2 STHE widespread use and its relatively more complex flow pattern compared to the heat exchangers having axial flow patterns. This method is herein referred to as Discrete Sub–Heat Exchanger (DSHE) method. Distinct from the original approach, the DSHE employs a defined NTU condition rather than a defined area condition for thermal analysis of the sub–heat exchanger pairs.

ARTICLE IN PRESS

Furthermore, unlike the method proposed by Karellas [29], the DSHE method can also be applied to the heat exchangers having multi–tube passes. More than what non– dimensional thermal analysis methods can offer, the DSHE approach facilitates the numerical calculation of effectiveness value, temperature profiles and heat distribution. This, as stated by Murty [34], thermal stresses of heat exchangers can be obtained from temperature profiles. In this way, head types can be selected for any shell–and–tube heat exchanger. In addition, it can be discovered from the heat distribution in which areas heat transfer augmentation measures can be taken. Moreover, with the DSHE method, effectiveness values of any flow patterns with more complex flow patterns can be also calculated numerically by considering only basic flow types. Within the scope of this research, two case studies, one exhibiting temperature cross and one without, are investigated to evaluate the DSHE method. Finally, to validate the DSHE method in wide NTU and Cr ranges, comprehensive sensitivity analyses were conducted depending on the number of nodes on the logarithmic scale and an analytical error map was generated.

ARTICLE IN PRESS

2. Methodology

A discrete sub–heat exchanger method is developed for numerically obtaining temperature profiles, heat distribution and numerical effectiveness value of the E–type shell–and–tube heat exchanger having two–tube passes (E_2 STHE) in this research. The numerical scheme is shown in Fig. 2, and the heat exchanger is discretized into parallel and counter sub–heat exchanger pairs along the heat exchanger. The defined NTU and Cr conditions are accepted in the formulation of the DSHE method. Therefore, the assumptions valid in the ε–NTU method are also valid in the DSHE method:

- The heat exchanger is in the steady state flow regime.
- There is no heat loss and longitudinal heat transfer.
- The heat transfer surface areas are equal in each discrete sub–heat exchanger.
- The overall heat transfer coefficient and the heat capacity ratio are constant along the heat exchanger.

- Discrete sub–heat exchanger pairs have parallel and counter–flow patterns.

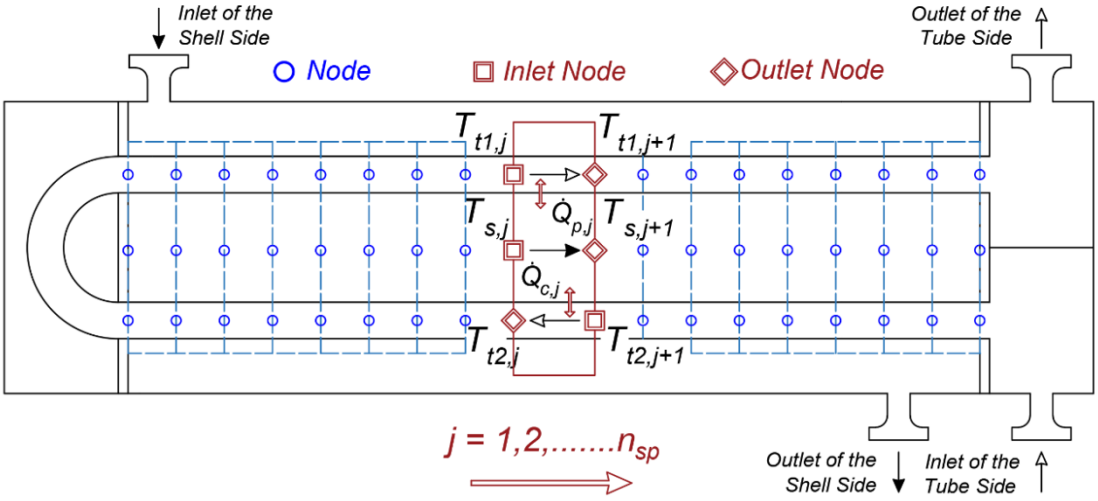


Fig. 2 DSHE schema of E_2 STHE

In Fig. 2, n_{sp} and j are the number of sub–heat exchanger pair and the index of a sub–heat exchanger pair, respectively. The temperature distribution and effectiveness value of E_2 STHE at defined NTU and Cr values are numerically calculated by applying the ε–NTU method iteratively to the sub–heat exchanger pairs having parallel and counter flow patterns. Thus, tube– and shell–side temperature vectors and the effectiveness value are updated with iterations. The ε– NTU method formulation applied to sub–heat exchanger pairs is shown in Eqs. 1–10. The number of transfer units (NTU) of sub–heat exchanger pairs is shown in Eq. 4.

$$C_{\min} = \min\left(C_t, C_s\right) \tag{1}$$

$$C_{\max} = \max\left(C_t, C_s\right) \tag{2}$$

$$C_r = \frac{C_{\min}}{C_{\max}} \tag{3}$$

$$ntu = \frac{NTU}{2\left(n_x - 1\right)} \tag{4}$$

ARTICLE IN PRESS

The effectiveness formulation of the sub–heat exchanger having a parallel flow pattern is shown in Eq. 5. If *Cr = 1*, the effectiveness formulation of the sub–heat exchanger having counter–flow pattern is shown in Eq. 6. If *Cr ≠ 1*, the effectiveness formulation of the sub–heat exchanger with counter flow pattern is shown in Eq. 7.

$$e_p = \frac{1 - \exp\left[-ntu(1+C_r)\right]}{1+C_r} \tag{5}$$

$$e_c = \frac{ntu}{1+ntu} \tag{6}$$

$$e_c = \frac{1 - \exp\left[-ntu(1-C_r)\right]}{1 - C_r \exp\left[-ntu(1-C_r)\right]} \tag{7}$$

While heat transfers in the sub–heat exchanger pairs with parallel and counter–flow patterns are shown in Eqs. 8 and 9, respectively, total heat transfer is shown in Eq. 10. In Eqs. 8 –10, *k*, which is superscript, is the iteration number.

$$\dot{Q}_{p,j}^{k} = e_p C_{min}\left(T_{s,j}^{k} - T_{t1,j}^{k}\right) \tag{8}$$

$$\dot{Q}_{c,j}^{k} = e_c C_{min}\left(T_{s,j}^{k} - T_{t2,j+1}^{k}\right) \tag{9}$$

$$\dot{Q}_{j}^{k} = \dot{Q}_{p,j}^{k} + \dot{Q}_{c,j}^{k} \tag{10}$$

After determining the heat transfers to the sub–heat exchanger pairs, the outlet temperatures are shown in Eqs. 11 – 13. Tube–side boundary condition for E_2 STHE is shown in Eq. 14.

$$T_{s,j+1}^{k} = T_{s,j s,j}^{k} - \frac{\dot{Q}_{j}^{k}}{C_s} \tag{11}$$

ARTICLE IN PRESS

ARTICLE IN PRESS

$$T_{t1,j+1}^{k} = T_{t1,j}^{k} - \frac{\dot{Q}_{p,j}^{k}}{C_t} \tag{12}$$

$$T_{t2,j}^{k} = T_{t2,j+1}^{k} - \frac{\dot{Q}_{c,j}^{k}}{C_t} \tag{13}$$

$$T_{t1,1}^{k} = T_{t2,1}^{k} \tag{14}$$

After calculating the outlet temperatures of each sub–heat exchanger pairs, total heat transfers and effectiveness of the heat exchanger is calculated by using Eqs. 15 and 16. The total heat transfer value for the tube–side is shown in Eq. 17, while the total heat transfer value for the shell–side is shown in Eq. 18. Due to the conservation of energy, the heat transfer values shown in Eqs. 15 and 16 are expected to be equal. However, due to the nature of numerical methods, a certain margin of error is always present. For this reason, as shown in Eq. 17, the total heat transfer is accepted as the average of the values in Eqs. 15 and 16. As a result, the effectiveness value of the heat exchanger can be calculated numerically, as shown in Eq. 18.

$$\dot{Q}_{t}^{k} = C_t\left(T_{t,outlet}^{k} - T_{t,inlet}^{k}\right) \tag{15}$$

$$\dot{Q}_{s}^{k} = C_s\left(T_{s,inlet}^{k} - T_{s,outlet}^{k}\right) \tag{16}$$

$$\dot{Q}^{k} = 0.5\left(\dot{Q}_{t}^{k} + \dot{Q}_{s}^{k}\right) \tag{17}$$

$$e_{num}^{k} = \frac{\dot{Q}^{k}}{C_{min}\left(T_{t,outlet} - T_{t,inlet}\right)} \tag{18}$$

Eqs. 19 and 20 show the analytical effectiveness formulation of the E_2 STHE and the analytical error rate of the DSHE, respectively.

$$e_{analy} = \frac{2}{\left(1+C_r\right)+\sqrt{1+C_r^2}\coth\left(\frac{NTU\sqrt{1+C_r^2}}{2}\right)} \text{ [2]} \tag{19}$$

$$e_{r,A}^{k} = \frac{\left|e_{num}^{k} - e_{analy}\right|}{e_{analy}} \tag{20}$$

Due to the iterative and discrete nature of the DSHE formulation, the total heat transfer rates calculated from the tube side and shell side are not exactly identical at sub–iterations. To ensure consistency with the first law of thermodynamics, a conservation of energy verification is performed at each iteration by monitoring the relative difference between tube– and shell–side heat transfer rates. This difference is quantified using the first–law error rate ($e_{r,\mathrm{I}}$), defined as the normalized difference between the two heat transfer values. The solution is considered to be in accordance with the first law of thermodynamics when $e_{r,\mathrm{I}}$ decreases below a prescribed tolerance. In this study, the total heat transfer rate is therefore taken as the average of the tube– and shell–side values, which reduces numerical bias while preserving overall energy balance.

$$e_{r,I}^{k} = \frac{\left|\dot{Q}_t^{k} - \dot{Q}_s^{k}\right|}{\dot{Q}_s^{k}} \tag{21}$$

In addition, the tube– and shell–side outlet temperatures, and their error rates are also shown in Eqs. 22–25.

$$T_{t,outlet}^{k+1} = T_{t1,end}^{k} \tag{22}$$

$$T_{s,outlet}^{k+1} = T_{s,end}^{k} \tag{23}$$

$$e_{r,Tt}^{k} = \frac{\left|T_{t,outlet}^{k+1} - T_{t,outlet}^{k}\right|}{T_{t,outlet}^{k+1}} \tag{24}$$

$$e^{k}_{r,Ts} = \frac{\left| T^{k+1}_{s,outlet} - T^{k}_{s,outlet} \right|}{T^{k+1}_{s,outlet}} \quad (25)$$

The numerical accuracy of the DSHE method depends on the number of sub–heat exchanger pairs (n_{sp}) used to represent the heat exchanger. Increasing n_{sp} improves spatial resolution but it also increases computational cost and the number of iterations required for convergence. To prove this, a node sensitivity (grid independence) study will be conducted in the Results and Discussion section.

3. Results and Discussion

The analysis results of the DSHE method developed for the E_2 STHE will be discussed with two study cases from the literature in this research. In the first study case examined, temperature variations were relatively lower, while in the second case, the opposite was true. This is to demonstrate the numerical robustness of the DSHE method. For the first case study, the case study was conducted from Sekulic et al. [2]. For the second case study, the case study was conducted by Teke et al. [35]. In the first study case, temperature variations are relatively small, and there is no temperature cross [2]. However, in the second case study, the temperature changes are dramatic and a temperature cross is present. Table 1 presents the thermal parameters for both case studies. Moreover, the parameters about to converge are shown in Table 2.

ARTICLE IN PRESS

Table 1. The Thermal Parameters of the Study Cases

	C_t kW/K	**C_s** kW/K	**C_r**	**NTU**	**$T_{s,inlet}$** °C	**$T_{t,inlet}$** °C
Case 1	75.7847	76.0122	0.9970	0.1852	63	35
Case 2	31.8136	15.9068	0.50	3.4	35	10

Table 2. The Converge Parameters

ARTICLE IN PRESS

Converge Parameter	Converge Criterion	Number of Node	Max Iteration Number
$e_{r,I}$	10^{-8}	10^{4}	10^{5}

The sensitivity analyses based on n_{sp} will also be carried out for the case studies. Finally, the analytical error rate map will be generated and interpreted for defined NTU and Cr ranges at the same inlet temperatures and C_{min} values with Case Study 2. As additional information, the DSHE method modeling and analyses were performed in the MATLAB environment [36].

3.1 Temperature Profile, Heat Distribution and Numerical Effectiveness Values

For the study cases, the analytical and numerical effectiveness values are shown in Table 3, comparatively. In both cases, the DSHE method has given precise results for effectiveness values with this flow pattern. As can be noted, the analytical error rate of Case 1, which has a lower NTU value, is lower than Case 2. Temperature profile, error rates, heat distribution and outlet temperatures from the DSHE analysis for the case studies are shown in Figs. 3 and 4, respectively.

ARTICLE IN PRESS

Table 3. The Analytical and Numerical Effectiveness Values

	Case 1	Case 2
$\boldsymbol{\varepsilon_{analy}}$	0.155547	0.74930
$\boldsymbol{\varepsilon_{num}}$	0.155548	0.74931
$\boldsymbol{e_{r,A}}$	3.87e–06	1.25e–06

The temperature profile is shown in Fig. 3a and usual for the flow pattern of the E_2 STHE. In Fig. 3b, the error rates calculated during the numerical convergence process are presented. First law error rate ($e_{r,I}$) represents the solution accuracy in terms of energy conservation. Analytical error rate ($e_{r,A}$) represents relative difference between analytical and numerical effectiveness values while the other error rates ($e_{r,Tt}$, $e_{r,Ts}$) represents relative difference of outlet temperatures between successive iterations. While all error rates decrease with iterations, however, $e_{r,I}$ converges later and $e_{r,A}$ follows a

horizontal trend after a certain number of iterations. This indicates that the DSHE model has reached solution stability and it is appropriate to prefer er_I as a convergence parameter. The heat distribution is illustrated in Fig. 3c. Total discrete heat transfer decreases along the shell–side fluid flow direction. From this, it can be concluded that the average temperature difference decreases through this direction. Moreover, the difference between discrete parallel and counter heat transfers increases through this direction. Fig. 3d shows that the outlet temperatures stabilize after a certain number of iterations.

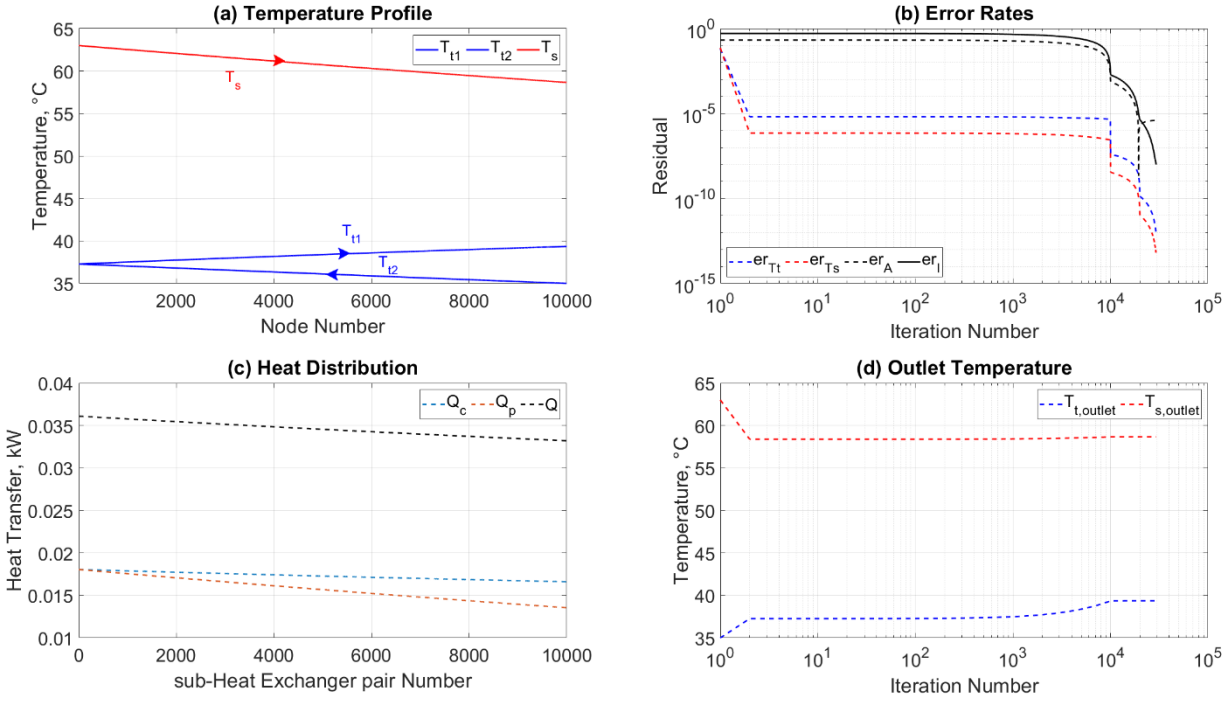


Fig. 3 *The Results for Case 1*

The temperature profile of Case 2, which is the DSHE analysis result, is shown in **Fig. 4a,** and the temperature cross can be observed. Note that the temperature changes are greater compared to Case 1 due to the higher *NTU* value. After a certain node, the temperature of the tube–side fluid exceeds the temperature of the shell–side fluid. This indicates that the reverse heat transfer mechanism is carried out in the heat exchanger. Moreover, after the temperature cross, discrete parallel heat transfer turns from positive to

negative after temperature cross, as seen Fig. 4c. As a result, the derivative of the tube–side fluid temperature curve also turns from positive to negative. However, despite the reverse heat transfer mechanism, the sign of the derivative of the shell–side fluid didn't change. The general trends of the error rate curves in Fig. 4b are similar to those in Fig. 3b. However, $e_{r,A}$ stabilizes at a higher level. In the other words, the final analytical error value is obtained than that of Case 1. Fig. 4c shows the heat distribution of Case 2, one of the DSHE analysis results. Unlike Case 1, after a certain point the discrete sub–parallel heat transfer turns from positive to negative due to the temperature cross. This clearly reveals the reverse heat transfer after the temperature cross point. This reverse heat transfer effect becomes more pronounced as it progresses along the shell–side. Fig. 4d shows that the outlet temperatures and a similar convergence trend as Case 1 is observed, but more iterations are required.

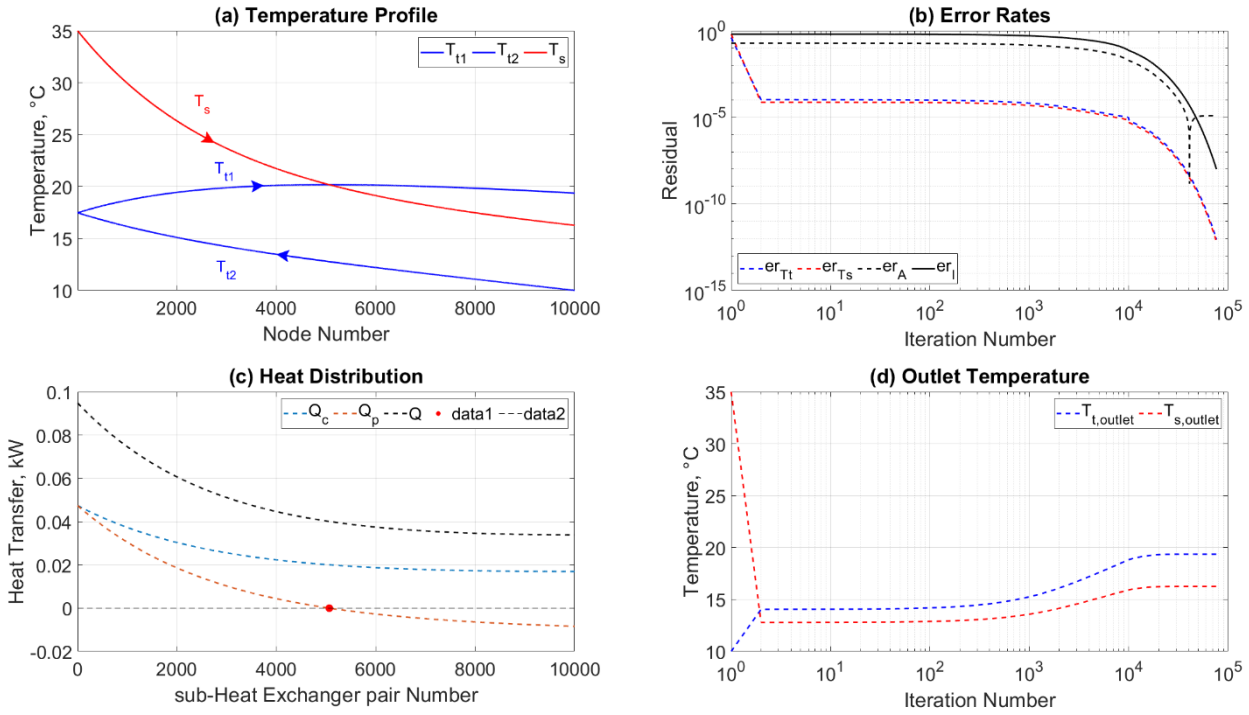


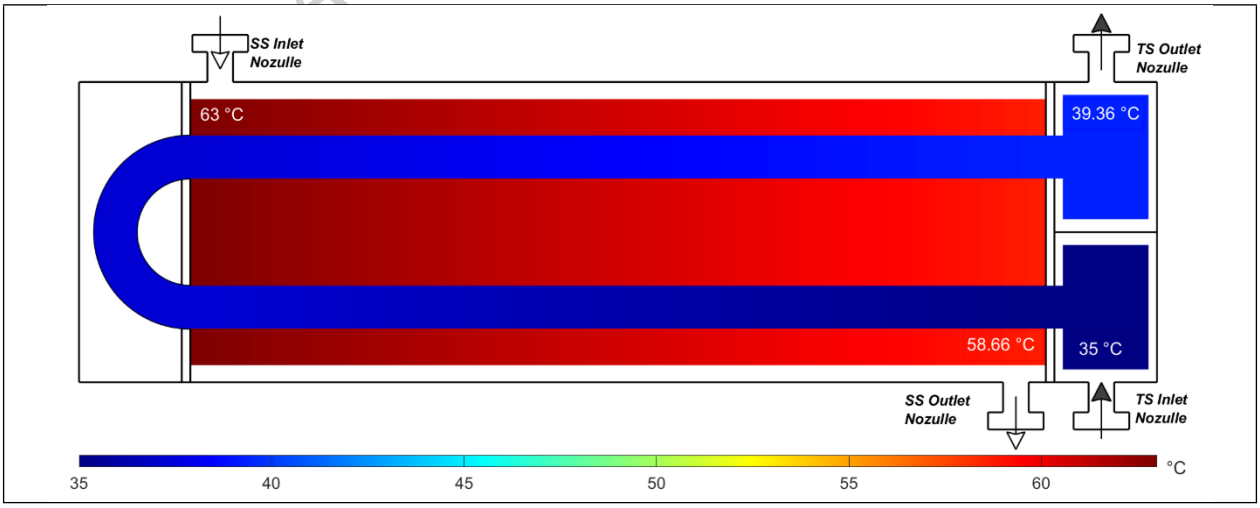
Fig. 4 *The Results for Case 2*

In these case studies, the convergence is enforced using a strict first–law error criteria of 10^{-8}, which ensures that energy conservation is satisfied

within numerical precision. The analytical error and outlet temperature error curves observed in the Results section reach a stable lower bound after a sufficient number of iterations; this behavior reflects the combined effect of discretization and floating point precision rounding rather than insufficient iterations. Additional iterations beyond this point do not produce meaningful changes in the calculated effectiveness or temperature profiles. Therefore, the reported numerical results are considered numerically stable, and DSHE uncertainty is dominated by discretization resolution rather than convergence tolerance.

Fig. 5 presents the temperature maps obtained from the results of the DSHE analysis for both cases. These maps visually represent tube– and shell–side temperatures along the discrete nodes for both the cases. In Fig. 5a for Case 1, the temperature gradients are quite moderate than that of Case 2, and no temperature cross is observed. In Fig. 5b for Case 2, the temperature map has much more pronounced gradients, and the temperature cross is clearly visible. After a certain node, tube–side fluid temperature exceeds shell–side temperature due to temperature cross. Thanks to these maps, the performance of the heat exchanger can be monitored not only by numerical values but also by one–dimensional spatial trends.

ARTICLE IN PRESS



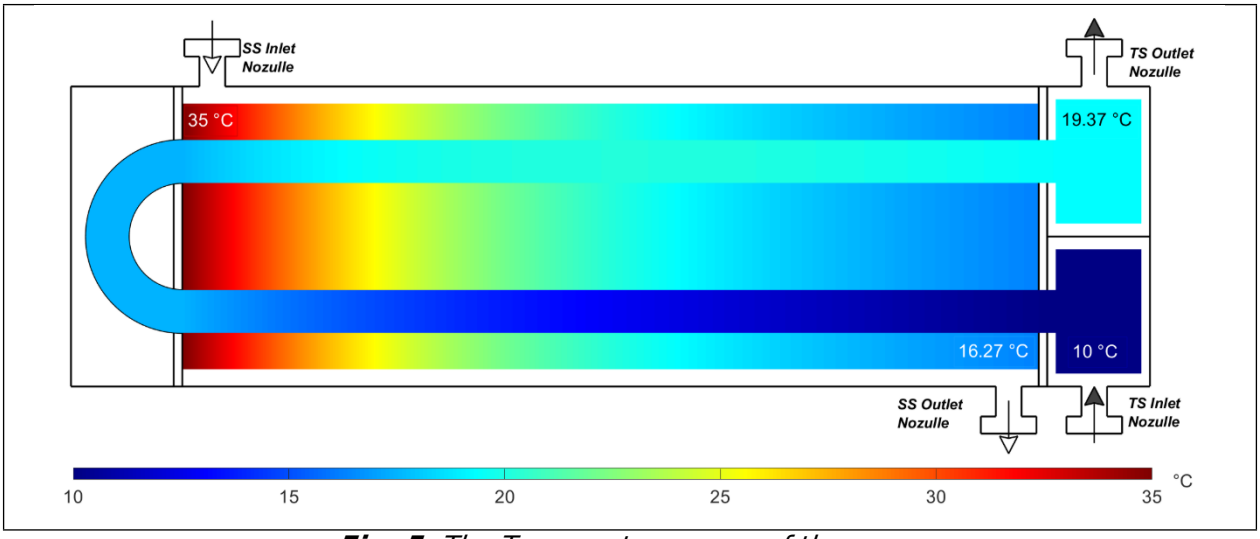


Fig. 5. *The Temperature maps of the cases*

Fig. 6 represents the heat maps along the heat exchanger for both cases. These maps visually represent the discrete sub–heat transfers, shown in Eqs. 8–10, calculated from the results of the DSHE analysis. In the heat map shown in Fig. 6a for Case 1, it can be noticed that the heat distribution along the heat exchanger is moderate. The color distribution is close to homogeneous and the heat transfer is larger in the inlet regions where there is a high temperature difference. In Fig. 6b, the color distribution is more varying than that of Case 1, and negative heat transfer is observed in some regions (shown in dark blue colors in the figure). These negative values are the regions where the temperature cross occurs and clearly indicate the reverse heat transfer mechanism. This phenomenon is consistent with the positive to negative heat transfer trends observed in sub–heat exchangers having parallel flow. Since these maps show in detail the direction and magnitude of heat exchange occurring in different regions of the system, they make it easier for designers to identify temperature cross, critical region or pinch point.

ARTICLE IN PRESS

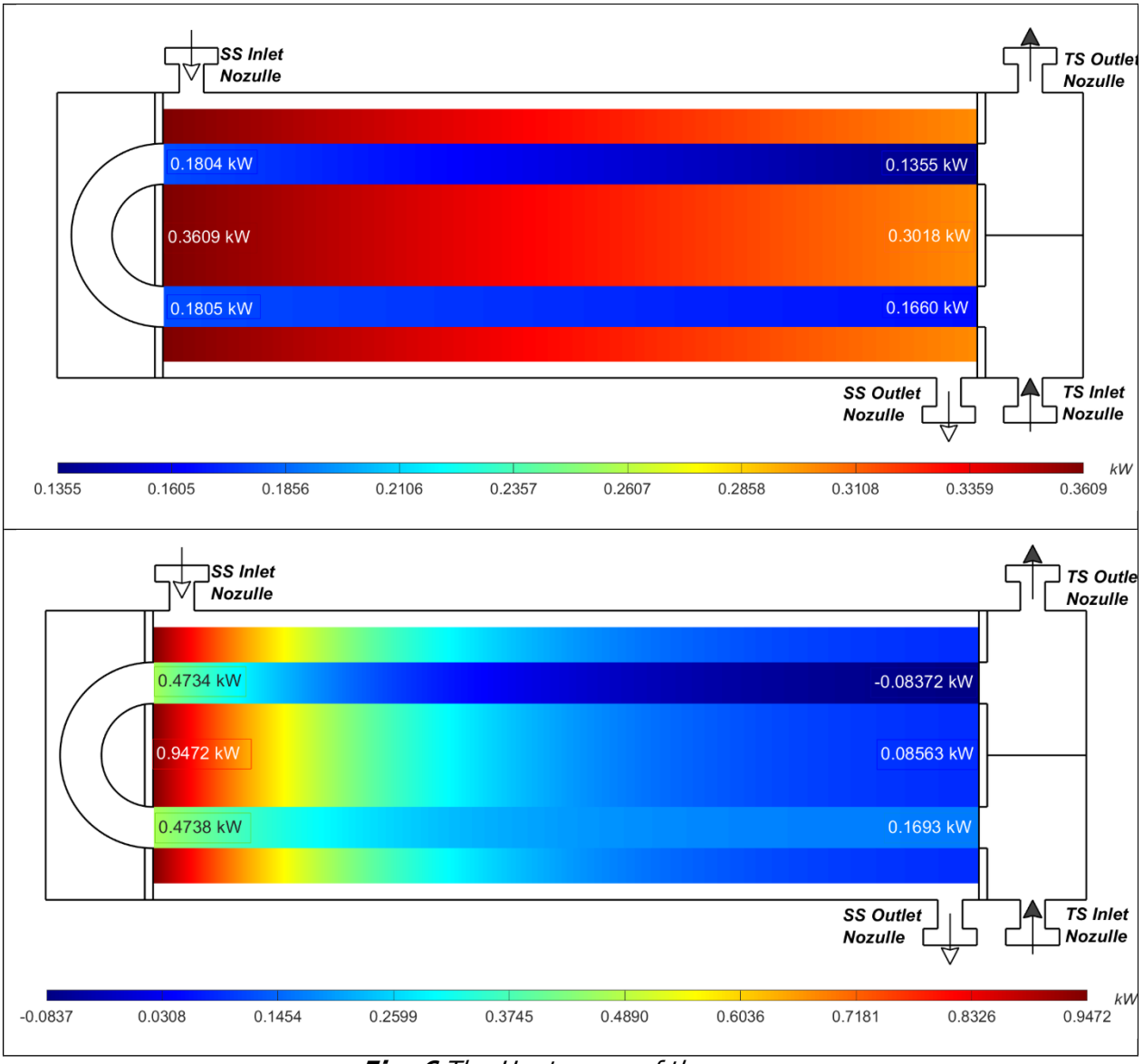


Fig. 6 *The Heat maps of the cases*

3.2. Sensitivity Analyses and Error Map

Analytical error rate curves at different numbers of nodes are shown in Figs. 7a and 7b for Cases 1 and 2, respectively. According to the results, the final analytical error rate values decrease linearly with the increase in the number of nodes on a logarithmic scale. The opposite is true for the number of iterations. As an additional knowledge, single program multiple data (*spmd*) [37], is applied to the DSHE method at 10^3 and 10^6 n_{sp} to reduce the computational time. Moreover, the relationship between final analytical error rates and numbers of nodes are also shown in Fig. 7c for both cases and the

same situation applies here. It can be seen that the second case study, having higher NTU value, has higher analytical error rates. It may be considered whether a similar situation exists for Cr, the other non–dimensional parameter for the effectiveness of the heat exchangers. For this reason, it may be useful to examine Fig. 8.

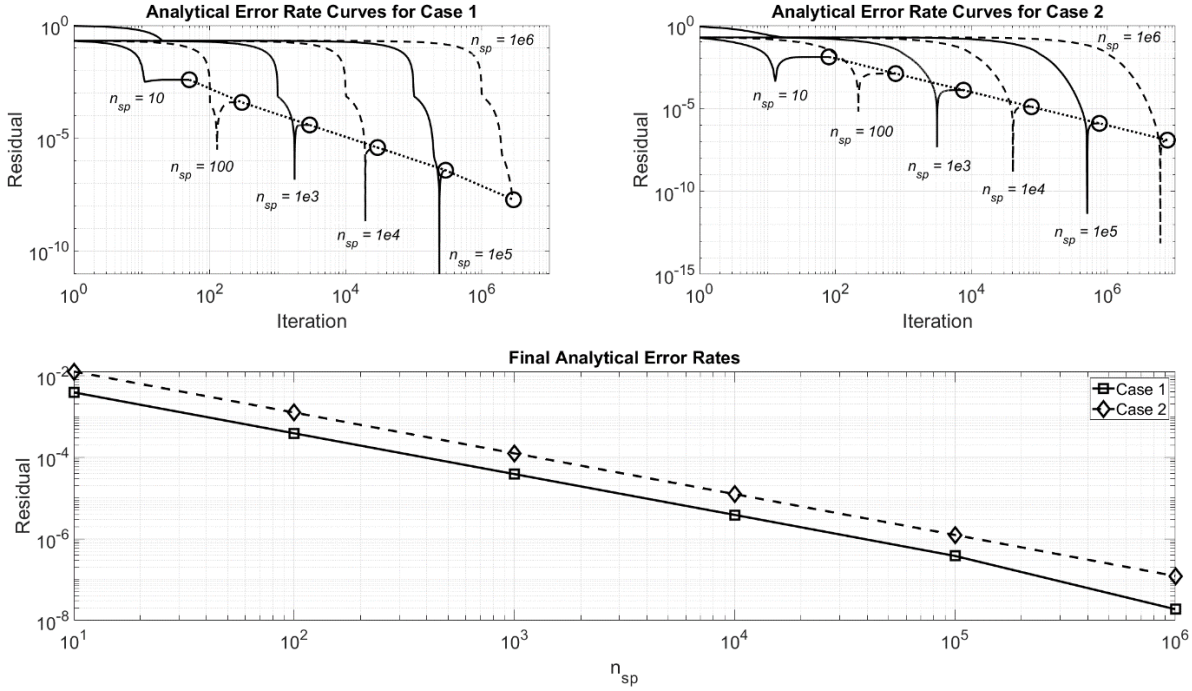


Fig. 7 *Sensitivity analyses*

Eqs. 26 and 27 demonstrated the regressions describing the relationship between n_{sp} and er_A for Case 1 and 2, respectively. The coefficient of determination (r^2) is *0.9977* for Case 1 and *0.999998* for Case 2.

$$er_A = \exp\left(-1.046153441978004 \times \ln\left(n_{sp}\right) - 3.000350249451369\right) \quad (25)$$

$$er_A = \exp\left(-1.002394403739722 \times \ln\left(n_{sp}\right) - 2.060488246567649\right) \quad (26)$$

Fig. 8 demonstrates the relationship between the computation times of the DSHE method modeled with *spmd* and the number of sub–heat exchanger pairs for both case studies. As can be seen from the figure, the computation time (wall clock time) has a linear relationship with nsp on a logarithmic scale.

ARTICLE IN PRESS

The computer processor used for the analyses is an *AMD R9 5900x* [38] and it uses 20 threads.

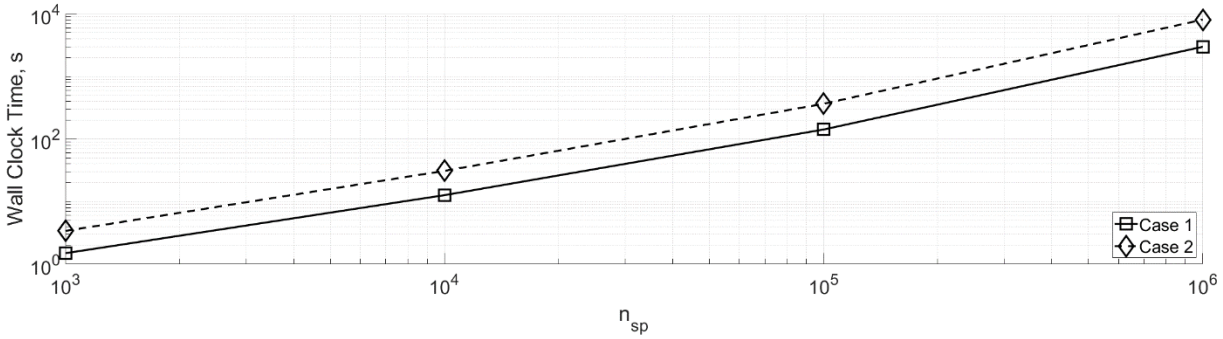


Fig. 8 *Wall Clock Time with spmd Modelling*

The analytical error rate surface map, depending on *NTU* and *Cr*, presented in Fig. 9, shows that high NTU and Cr values increase the error rate values. For this reason, increasing the number of nodes at high NTU and Cr values is important to maintain the accuracy of the DSHE analysis. However, it should not be forgotten that a high number of nodes also brings high computation times as a cost. Therefore, the use of algorithm acceleration methods such as *spmd* in the DSHE can be considered as a solution to reduce the computational time in the DSHE analyses.

ARTICLE IN PRESS

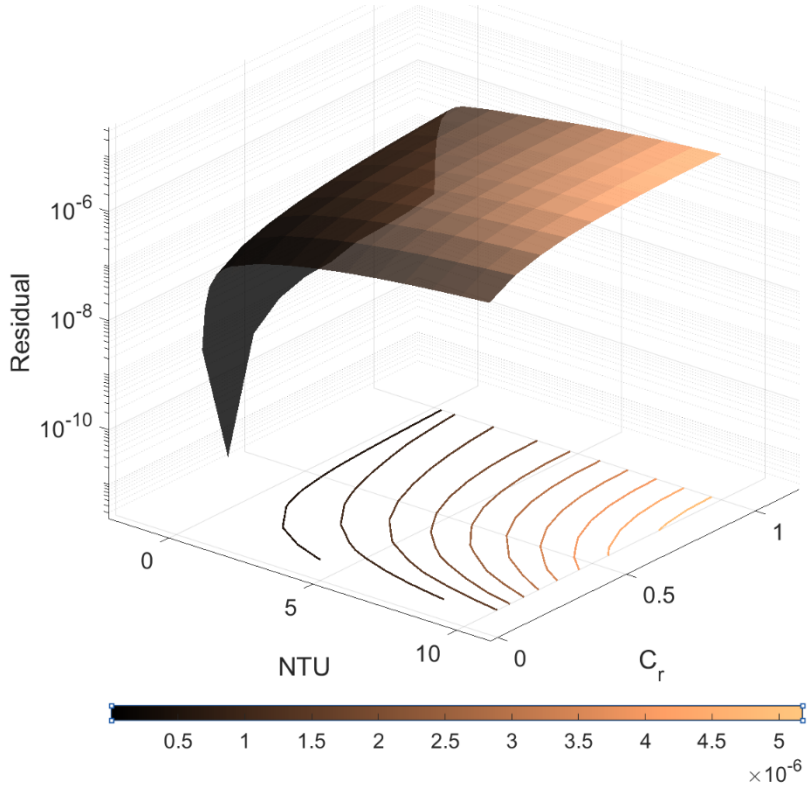


Fig. 9 *Analytical Error Rate Map*

4. Conclusion

This research introduced the Discrete sub–Heat Exchanger method with applying on E–type shell–and–tube heat exchangers having two–tube passes by considering only axial–flow patterns. The method successfully provided detailed temperature profiles and heat distributions across the heat exchanger profile, while also accurately computing the heat exchanger's effectiveness at defined NTU and Cr values, even in the presence of temperature cross. The key findings from the analysis are as follows:

- The DSHE method enables visualization of temperature and heat maps across the heat exchanger profile.
- A reverse heat transfer mechanism can appear when a temperature cross occurs.
- Among all error rates, the first law error rate is the most reliable convergence parameter.

ARTICLE IN PRESS

- Analytical error rate follows a horizontal trend after a certain number of iterations, establishing a lower limit influenced by the number of sub–heat exchanger pair (n_{sp}).
- As the number of sub–heat exchanger pairs increases, the number of iterations increases while the final analytical error rate decreases linearly on the logarithmic scale.
- As the number of sub–heat exchanger pairs increases, the computational time increases linearly on the logarithmic scale.
- Higher NTU and Cr values correlate with increased the final analytical error rate and number of iteration at constant the number of sub–heat exchanger pairs. The error rates vary on the order of 10^{-5} to 10^{-11} within the defined NTU and Cr ranges.

Future work may extend the DSHE to more complex flow patterns, such as divided–flow shell–and–tube heat exchangers, and apply it to trans–critical or two–phase flow scenarios. However, for longitudinal wall heat conduction or unsteady thermal analyses, the finite difference or finite volume methods can be proposed. Additionally, adopting alternative algorithm acceleration techniques could further enhance the computational efficiency of the DSHE method.

ARTICLE IN PRESS

DECLARATIONS

Ethical Approval

There are no human or animal studies in this research.

Competing interests

The authors declare that they have no known competing financial interests or personal relationships that could have appeared to influence the work reported in this paper.

Authors' contributions

Kubilay Bayramoglu: Supervisor, Writing–Reviewing and Editing

İbrahim KAYA: Conceptualization, Methodology, Modelling, Visualization, Investigation

Yasin ÜST: Data Curation, Writing–Original draft preparation

Funding

There is no funding received.

Data Availability

All data generated or analyzed during this study are included in this published article. No external datasets were used.

References

[1] W.M. Kays, A.L. London, Compact Heat Exchangers, 3rd ed., McGraw-Hill, 1984.

[2] R.K. Shah, D.P. Sekuli, Fundamentals of Heat Exchanger Design, 2007. https://doi.org/10.1002/9780470172605.ch10.

[3] X. Hu, P. Chen, X. Guo, X. Zhang, Comparative studies on the thermal performance of novel PCM-based heat sinks using 3D-printed thermal conductivity enhancers, Int. Commun. Heat Mass Transf. 162 (2025) 108613. https://doi.org/10.1016/j.icheatmasstransfer.2025.108613.

[4] X. Hu, P. Chen, X. Guo, X. Zhang, Numerical investigation on thermal behavior of PCM embedded in structured porous fins (SPFs) with various configurations and materials, Appl. Therm. Eng. 274 (2025) 126617. https://doi.org/10.1016/j.applthermaleng.2025.126617.

[5] A.A. Delouei, H. Sajjadi, R. Mohebbi, M. Izadi, Ultrasonics - Sonochemistry Experimental study on inlet turbulent flow under ultrasonic vibration : Pressure drop and heat transfer enhancement, Ultrason. - Sonochemistry 51 (2019) 151–159. https://doi.org/10.1016/j.ultsonch.2018.10.032.

[6] A.A. Delouei, H. Sajjadi, M. Izadi, R. Mohebbi, The simultaneous e ff ects of nanoparticles and ultrasonic vibration on inlet turbulent fl ow : An experimental study, 146 (2019) 268–277. https://doi.org/10.1016/j.applthermaleng.2018.09.113.

[7] A. Amiri, H. Naeimi, H. Sajjadi, M. Atashafrooz, An active approach to heat transfer enhancement in indirect heaters of city gate stations : An experimental modeling, Appl. Therm. Eng. 237 (2024) 121795. https://doi.org/10.1016/j.applthermaleng.2023.121795.

[8] A.A. Delouei, H. Sajjadi, G. Ahmadi, The Effect of Piezoelectric Transducer Location on Heat Transfer Enhancement of an Ultrasonic - Assisted Liquid - Cooled CPU Radiator, Iran. J. Sci. Technol. Trans. Mech. Eng. 48 (2024) 239–252. https://doi.org/10.1007/s40997-023-00667-5.

[9] A. Jalali, A.A. Delouei, M.R. Zaertaraghi, S.A. Tavasoli, Experimental Investigation on Active Heat Transfer Improvement in Double-Pipe Heat Exchangers, (2024).

ARTICLE IN PRESS

[10] Tubular Exchanger Manufacturers Association (TEMA), (2024). https://tema.org/.

[11] D.P. Sekulić, R.K. Shah, A. Pignotti, A review of solution methods for determining effectiveness-NTU relationships for heat exchangers with complex flow arrangements, Appl. Mech. Rev. 52 (1999) 97–117. https://doi.org/10.1115/1.3098928.

[12] A.J. V. Underwood, The calculation of the mean temperature difference in multi-pass heat exchangers, J. Inst. Pet. Technol. 25 (1934).

[13] W.M. Nagle, Mean Temperature Differences in Multipass Heat Exchangers, Ind. Eng. Chem. 25 (1933) 604–609. https://doi.org/10.1021/ie50282a003.

[14] Donald Q. Kern, Process Heat Transfer.Pdf, (1950) 871. http://sv.20file.org/up1/423_0.pdf.

[15] F.K. Fischer, Mean Temperature Difference Correction in Multipass Exchangers, Ind. Eng. Chem. 30 (1938) 377–383. https://doi.org/10.1021/ie50340a004.

[16] B.Y.R.A. Bowman, A.C. Mueller, W.M. Nagle, Mean Temperature Difference in Design, (1940).

[17] Çengel Yunus A., Book - Heat and Mass Transfer Fundamentals and Applications 5Th, 2007.

[18] D. KERN, A. KRAUS, The effectiveness of heat exchangers with one shell pass and even numbers of tube passes, ASME 65 (1965).

[19] B.S. Baclic, 1-2 N shell-and-tube exchanger effectiveness: a simplified Kraus-Kern equation, J. Heat Transf. (Transcations ASME (American Soc. Mech. Eng. Ser. C);(United States) 111 (1989).

[20] B.S. Bačlić, 1-(2N-1) shell-and-tube exchanger effectiveness: Explicit equations, Heat Mass Transf. Und Stoffuebertragung 33 (1997) 163–165. https://doi.org/10.1007/s002310050174.

[21] R.A. Seban, Multipass Heat Exchangers With a Single Well-Mixed Shell Pass, J. Heat Transfer 110 (1988) 782–785. https://doi.org/10.1115/1.3250560.

[22] A. Pignotti, P.I. Tamborenea, Thermal effectiveness of multiple shell and tube pass TEMA E heat exchangers, J. Heat Transfer 110 (1988) 54–59. https://doi.org/10.1115/1.3250472.

[23] J.D. Domingos, Analysis of complex assemblies of heat exchangers, Int. J. Heat Mass Transf. 12 (1969) 537–548. https://doi.org/10.1016/0017-9310(69)90037-4.

[24] A. Pignotti, Matrix formalism for complex heat exchangers, J. Heat

ARTICLE IN PRESS

Transfer 106 (1984) 352–360. https://doi.org/10.1115/1.3246680.

[25] R. Crozier, M. Samuels, Mean temperature difference in odd-tube-pass heat exchangers, J. Heat Transfer 99 (1977) 487–489. https://doi.org/10.1115/1.3450724.

[26] M.S. O'Hare, L. Hess, A.D. Kraus, The effectiveness of heat exchangers with one shell pass and an odd number of tube passes, in: Int. Heat Transf. Conf. Digit. Libr., Begel House Inc., 1986.

[27] E.S. Gaddis, E.U. Schlünder, Temperature distribution and heat exchange in multipass shell-and-tube exchangers with baffles, Heat Transf. Eng. 1 (1979) 43–52. https://doi.org/10.1080/01457637908939548.

[28] R.J. Ribando, G.W. O'Leary, S. Carlson-Skalak, General numerical scheme for heat exchanger thermal analysis and design, Comput. Appl. Eng. Educ. 5 (1997) 231–242.

[29] S. Karellas, A. Schuster, A.D. Leontaritis, Influence of supercritical ORC parameters on plate heat exchanger design, Appl. Therm. Eng. 33–34 (2012) 70–76. https://doi.org/10.1016/j.applthermaleng.2011.09.013.

[30] E. Cayer, N. Galanis, M. Desilets, H. Nesreddine, P. Roy, Analysis of a carbon dioxide transcritical power cycle using a low temperature source, Appl. Energy 86 (2009) 1055–1063. https://doi.org/10.1016/j.apenergy.2008.09.018.

[31] M. Li, J. Wang, S. Li, X. Wang, W. He, Y. Dai, Thermo-economic analysis and comparison of a CO2 transcritical power cycle and an organic Rankine cycle, Geothermics 50 (2014) 101–111. https://doi.org/10.1016/j.geothermics.2013.09.005.

[32] S. Bracco, I. Faccioli, M. Troilo, Dynamic Simulation Model of a Two-Fluids Heat Exchanger Based on a Numerical Discretization Method, (2007) 285–293.

[33] G. Nellis, S. Klein, Heat Transfer, Cambridge University Press, New York, 2009.

[34] K.N. Murty, Heat transfer characteristics of one-and two-tube-pass split-flow heat exchangers, Heat Transf. Eng. 4 (1983) 26–34. https://doi.org/10.1080/01457638108939606.

[35] I. Teke, Ö. Ağra, H. Demir, S.Ö. Atayilmaz, Sizing, selection, and comparison of heat exchangers considering the lowest saving-investment ratio corresponding to the area at the tag end of the heat exchanger, Energy 78 (2014) 114–121. https://doi.org/10.1016/j.energy.2014.08.035.

ARTICLE IN PRESS

[36] MathWorks Matlab, (2024). https://www.mathworks.com/.

[37] Single Program Multiple Data, (2024). https://www.mathworks.com/help/parallel-computing/spmd.html.

[38] AMD cpu properties, (2025). https://www.amd.com/en/products/processors/desktops/ryzen/5000-series/amd-ryzen-9-5900x.html.

Nomenclature

	Symbols		***Subscripts***
C	Heat capability [W/K]	***anal y***	Analytical
Cr	Heat capability ratio	***min***	Minimum
N_p	Number of Tube Passes	***max***	Maximum
n	Number	***sp***	sub–Heat Exchanger pair
ntu	Number of Transfer Units of sub–Heat Exchanger	***r***	Rate
NTU	Number of transfer units	***p***	Parallel
$\dot{Q}$	Heat transfer rate [W]	***c***	Counter
T	Temperature [°C]	***j***	Counter
e	Error Rate	***t***	Tube – Side
P	Thermal Effectiveness	***s***	Shell – Side
R	Heat capability ratio	***num***	Numerical
F	Correction Factor	***I***	First Law
	Abbreviations		***Superscript***
DSHE	Discrete sub – Heat Exchanger	***k***	Iteration Number
E_2 ***STHE***	E–type shell–and–tube heat exchanger having two–tube passes		***Greek Symbols***
TEMA	Tubular Exchanger Manufacturers Association	ε	Effectiveness
SS	Shell – Side Fluid		

ARTICLE IN PRESS

TS	Tube – Side Fluid		
LMTD	Logarithmic Temperature Mean Difference		
spmd	Single Program, Multi Data		

ARTICLE IN PRESS